Catalysis Today 170 (2011) 126–133

Contents lists available at ScienceDirect

Catalysis Today

journal homepage: www.elsevier.com/locate/cattod

Rotating disc electrode studies of borohydride oxidation at Pt and bimetallic Pt–Ni and Pt–Co electrodes

A. Tegou[a], S. Papadimitriou[a], I. Mintsouli[a], S. Armyanov[b], E. Valova[b], G. Kokkinidis[a], S. Sotiropoulos[a,*]

[a] Department of Chemistry, Aristotle University of Thessaloniki, Thessaloniki 54124, Greece
[b] Rostislaw Kaischew Institute of Physical Chemistry, Bulgarian Academy of Sciences, Sofia 1113, Bulgaria

ARTICLE INFO

Article history:
Received 27 October 2010
Received in revised form 4 January 2011
Accepted 5 January 2011
Available online 2 February 2011

Keywords:
Platinum catalysts
Bimetallic catalysts
Galvanic replacement
Borohydride oxidation

ABSTRACT

The electrochemical oxidation of borohydride has been studied by means of voltammetry at Pt and Pt–Ni, Pt–Co bimetallic rotating disc electrodes (RDEs). The bimetallic catalysts are prepared by means of a galvanic replacement method (whereby electrodeposited Ni and Co layers are partially replaced by Pt when immersed in a chloroplatinic solution) and are shown to have a Pt shell–bimetallic alloy core. The effects of electrode history, potential scan direction, rotation speed and electrode material on borohydride oxidation have been investigated. For all Pt-based catalysts tested a gradual decrease of the voltammetric current from its initial value to a steady state response is observed in the kinetic control potential region, irrespective of scan direction and rotation speed. The initial deactivation of the catalyst at low overpotentials as well as the shape of the initial and steady-state voltammograms in that region point to the heterogeneous hydrolysis of borohydride and the subsequent oxidation of its products. As the catalytic activity for the hydrolysis reaction decreases the voltammograms shift to more positive potentials where direct borohydride oxidation dominates. The bimetallic Pt–Ni and Pt–Co catalysts exhibit a more negative open circuit potential and higher oxidation currents at low overpotentials than Pt, but lower apparent number of electrons transferred in the mass transport control region. These findings can be interpreted by the lowering of the d-band energy level of Pt in the presence of Ni and Co and the associated decrease in its adsorption affinity.

1. Introduction

Although the electrochemical oxidation of borohydride has long been studied and identified as a potential source of energy in the electrochemical literature [1–5], it was not until the beginning of the last decade that it attracted interest again as the anode reaction of direct borohydride fuel cells, in particular for possible portable device applications [6–8].

Direct borohydride oxidation can occur via one of the following two overall reactions depending on the anode material [6–10]:

$$BH_4^- + 8OH^- - 8e^- \rightarrow BO_2^- + 6H_2O \quad (1)$$

$$BH_4^- + 4OH^- - 4e^- \rightarrow BO_2^- + 2H_2O + 2H_2 \quad (2)$$

The complete-8e reaction occurs at materials that have a low hydrogen adsorption/evolution affinity such as Au and Ag with the first step speculated to be that of electron transfer and formation of a borohydride radical that rapidly hydrolyses and looses a second electron to form monoborane:

$$BH_4^- - e^- \rightarrow BH_4^\bullet \quad (3)$$

$$BH_4^\bullet + OH^- \rightarrow BH_3^- + H_2O \quad (4)$$

$$BH_3^- - e^- \rightarrow BH_3 \quad (5)$$

The latter hydrolyses further and dimerizes to diborane which then undergoes a stepwise 6e oxidation involving a number of intermediates [5].

The partial-4e reaction is favoured at materials that have significant hydrogen adsorption affinity and/or hydrogen evolution activity such as Pt, Ni, Pd, etc. with the first step being that of dissociative chemisorption:

$$BH_4^- + 2M \rightarrow M\text{–}BH_3^- + M\text{–}H \quad (6)$$

Following that, and depending on the strength of the M–BH_3^- and M–H bonds as well as on electrocatalytic activity, either electrochemical oxidation or heterogeneous hydrolysis may take place. In the former case the sequence of reactions involves electron loss by

* Corresponding author. Tel.: +30 2310 997742; fax: +30 2310 443922.
E-mail addresses: eczss@chem.auth.gr, eczss@otenet.gr (S. Sotiropoulos).

0920-5861/$ – see front matter © 2011 Elsevier B.V. All rights reserved.
doi:10.1016/j.cattod.2011.01.003

boron hydrides and further formation of adsorbed atomic hydrogen [11,12]:

$$M\text{–}BH_3^- + OH^- - e^- \rightarrow BH_3OH^- + M\text{–}H \quad (7.1)$$

$$M + BH_3OH^- + OH^- - e^- \rightarrow BH_2(OH)_2^- + M\text{–}H \quad (7.2)$$

$$M + BH_2(OH)_2^- + OH^- - e^- \rightarrow BH(OH)_3^- + M\text{–}H \quad (7.3)$$

$$M + BH(OH)_3^- + OH^- - e^- \rightarrow B(OH)_4^- + M\text{–}H \quad (7.4)$$

In the case that the M–H bond is not too strong and/or the H electrooxidation activity of M is not high, then the adsorbed atomic H of (6) and (7) can recombine to form molecular H_2:

$$M\text{–}H + M\text{–}H \rightarrow H_2 + 2M \quad (8)$$

If all adsorbed H reacts in such a way then the overall electrooxidation reaction becomes that given in (2) and involves 4e; if, however, the oxidation of H also takes place:

$$M\text{–}H + OH^- - e^- \rightarrow M + H_2O \quad (9)$$

Then the reaction appears to involve more than 4e (this has been reported in some cases, e.g. for Pt and Pd [13]).

The heterogeneous hydrolysis of borohydride, that may occur in parallel with its electrochemical oxidation, starts with the boron-containing adsorbate of (6) reacting with H_2O and adsorbed atomic hydrogen recombination to give molecular H_2 and is completed by further hydrolysis [14–16]:

$$M\text{–}BH_3^- + H_2O \rightarrow BH_3OH^- + M\text{–}H \quad (10.1)$$

$$M\text{–}H + M\text{–}H \rightarrow H_2 \quad (10.2)$$

$$BH_3OH^- + H_2O \rightarrow BO_2^- + 3H_2 \quad (10.3)$$

Overall, both the partial electrooxidation (due to reaction (8)) and heterogeneous hydrolysis of borohydride (reaction (10)), lead to a number of electrons transferred $n < 8$ and hence to a decrease in its coulombic efficiency as a potential fuel. Unfortunately, metals at which the reaction follows the 8e path (e.g. Au, Ag) show low electrocatalytic activity-high overpotentials for borohydride oxidation, whereas metals that exhibit high electrocatalytic activity-lower overpotentials (e.g. Pt, Ni) are also characterised by partial oxidation and high hydrolysis rates. In search for optimized electrocatalysts that would show reasonable catalytic activity without extended loss of coulombic efficiency, bimetallic catalysts (mainly Pt-based) have been proposed (see for example [10,17,18,19]) or additives (thiourea) have been reported to suppress hydrolysis [9,11,20].

Another inherent limitation of the borohydride fuel reaching its full potential (even at materials of high catalytic activity) is that the formal reduction potential of reaction (1) is −1.24 V vs. SHE witch is around 400 mV more negative than the formal potential of hydrogen evolution [21] and as a result the open circuit potential is a mixed potential, defined by borohydride oxidation (anodic reaction) and hydrogen evolution (cathodic reaction). From the single metal catalysts tested, Ni was found to have the most negative open circuit potential value (−1.03 V vs. SHE [13]), whereas recently a novel Pt/Ti_2O [18] binary catalyst has apparently shown a rest potential which is lower than that of Pt (ca. −1.00 V vs. SHE [3]). In a previous publication we have reported that a new class of modified Pt catalysts, consisting of a Pt-shell and a Pt–M core (M: Cu, Fe, Co, Ni, Pb) and prepared by a galvanic replacement process [22–31], showed decreased cathodic hydrogen evolution activity [31]. The latter finding and associated trends were in agreement with the predictions of Density Functional Theory (DFT) calculations of the "d-band shift theory" [32,33] that hydrogen adsorption at Pt is attenuated by the presence of metals with a smaller Wigner–Seitz radius and electronegativity than Pt. Such Pt(M) systems should therefore be good candidates for borohydride oxidation at potentials closer to its thermodynamic potential.

From the above discussion it follows that there are three possible sources of hydrogen evolution during voltammetric studies of borohydride oxidation at Pt-based electrodes: cathodic hydrogen evolution, if the negative limit of the potential scan is more negative than the rest potential; hydrogen produced by heterogeneous hydrolysis; hydrogen as a by-product of partial electrochemical oxidation. The first source of hydrogen can be avoided by careful choice of the start potential at values positive to the rest potential. The other two sources cannot be eliminated but at least a reproducible H_2 profile could be established via the well-controlled mass transfer rates at a Rotating Disk Electrode (RDE). Despite this fact there is a rather limited number of RDE studies of bororohydride oxidation [10,34–38]. In fact careful inspection of most of the data at Pt-based electrodes [10,19,34,36] reveals the existence of negative currents and hence evidence of cathodic hydrogen evolution (that most likely affects the anodic scan that follows) and that the effect of electrode history and scan direction have barely been studied.

The aim of this work has been dual: the detailed study of borohydride oxidation at Pt-based RDEs and the testing of the electrocatalytic activity of bimetallic Pt(M) electrodes. Specific objectives have been: (i) the preparation of Pt(Ni) and Pt(Co) catalysts by galvanic replacement of electrodeposited Ni and Co layers on glassy carbon electrodes, GC, and their characterization by SEM, EDS, XRD; (ii) the study of electrode history, scan direction and rotation speed effects during borohydride oxidation (BOR) at a Pt RDE; (iii) the comparison of the electrocatalytic activity towards BOR of Pt and Pt(M) electrodes and its implications for the possible reaction mechanism.

2. Experimental

2.1. Preparation of Pt(Ni)/GC and Pt(Co) electrodes

Electrodeposition of Ni and Co on GC disc electrodes (5 mm diameter) was carried out from 0.01 M Ni sulfamate + 0.227 mM $NiCl_2$ +0.025 M H_3BO_3 deaerated solutions at −1.1 V vs. SCE and from 5 mM $CoCl_2 \cdot 6H_20$ + 0.1 M $MgSO_4 \cdot 7H_20$ + 0.1 M H_3BO_3 deaerated solutions at −1.00 V vs. SCE, respectively. The charge density passed during plating was 308 mC cm^{-2} for Ni and 353 mC cm^{-2} for Co deposits which, taking into account the corresponding current efficiencies (found by *gravimetric* analysis to be 98% and 93–97%, respectively) and the bulk density of the two metals [39], gives an estimate of 108 nm and 122 nm for the thickness of electrodeposited Ni and Co. The Ni/GC and Co/GC electrodes were then immersed in a 0.1 M HCl + 10^{-3} M K_2PtCl_6 solution for 30 min so that spontaneous Ni and Co replacement by Pt occurred:

$$2Ni/GC + PtCl_6^{2-} \rightarrow Pt(Ni)/GC + 2Ni^{2+} + 6Cl^- \quad (11)$$

$$2Co/GC + PtCl_6^{2-} \rightarrow Pt(Co)/GC + 2Co^{2+} + 6Cl^- \quad (12)$$

These reactions are thermodynamically favorable since the standard potentials of the Co^{2+}/Co and Ni^{2+}/Ni couples are −0.277 and −0.257 V vs. SHE, respectively, i.e. they are lower than the standard potential of the Pt(IV)Cl_6^{2-}/Pt couple (+0.744 V vs. SHE) [21].

2.2. Microscopic, spectroscopic and crystallographic characterisation of coatings

A JEOL JSM-5510 microscope was used for Scanning Electron Microscopy (SEM) and elemental analysis of the catalyst layers was carried out by the incorporated EDS system.

From test experiments with co-sputtered Pt–Co and Pt–Ni 100 nm thick coatings of known composition we have estimated

an error of ±2% in the atomic composition of the samples as determined by EDS.

A SIEMENS D5000 diffractometer with a carbon monochromator was employed for Grazing incidence X-ray Diffraction (GIXRD) characterization of the deposits, with the set of experimental parameters being: CuKα radiation (λ = 1.5406 nm); incidence angle $\theta = 1^\circ$; scanning angular interval 30°/100° (2θ) with a constant scanning step $\Delta(2\theta) = 0.02^\circ$; counting time of 2.4 s per step.

2.3. Electrochemical experiments

Three-compartment glass cells were used for electrochemical experiments which were performed with the help of an Autolab 100 (EcoChemie) workstation. The working electrode substrate was a glassy carbon (3 mm diameter) or a 2 mm diameter Pt RDE, controlled by a Taccusel EDI101T motor, the counter electrode was a Pt coil and a saturated calomel electrode (SCE) equipped with a luggin capillary served as the reference electrode. All working electrode potential values reported hereafter are referred to the SCE.

Different cells were used for each step in the sequence of electrochemical experiments so that contamination was kept at a minimum. These involved (a) the electrodeposition of Ni and Co, (b) electrochemical activation of Pt(Ni)/GC and Pt(Co)/GC electrodes (prepared by immersion of the Ni/GC and Co/GC into a Pt(IV) exchange solution) by repetitive potential scanning at 1 V s^{-1} in a 0.1 M $HClO_4$ solution between hydrogen and oxygen evolution, so that any un-coated Ni or Co is removed, (c) electrochemical surface characterisation of the Pt-based catalyst in clean deaerated 0.1 M $HClO_4$ solution and (d) RDE voltammetry at a 10 mV s^{-1} potential sweep rate in the 0.01 M $NaBH_4$ + 1 M NaOH solution.

2.4. Electrode materials and chemicals

Ni sulfamate (p.a. 99%) from Fluka, $NiCl_2$ (puriss > 97%) from Merck, $CoCl_2 \cdot 6H_2O$, $MgSO_4 \cdot 7H_20$ from Merck (p.a. 99%) and H_3BO_3 (puriss 98%) from Aldrich were used for the preparation of the Ni and Co deposition solutions. Pt exchange solutions were prepared with H_2PtCl_6 hexahydrate from Sigma–Aldrich (ACS reagent, ≥37.50% as Pt). Sodium borohydride puriss p.a. ≥ 96% was from Fluka.

The Taccusel EDI101T RDE incorporated a 3 mm diameter glassy carbon laboratory-made tip fabricated from glassy carbon 1 mm thick plates (Alfa Aesar) cut into discs and permanently fixed into Teflon. Similar discs were used in SEM/EDS experiments after having been sealed into glass tubes with the help shrinkable thermoplastic sleeves. Electrical contact between the disc and a current collector commercial wire inserted into the glass tube was achieved by mercury drops. The bulk Pt (2 mm diameter) RDE, used for comparison, was fabricated from a metal rod from Goodfellow Ltd; 99.95%. Large sample substrates used in GIXRD experiments (1.5 cm in diameter) were fit into a Teflon holder equipped with sealing O-rings and a brass current collector rod protected by a glass sleeve. After each set of experiments the electrodes were treated with aqua regia to ensure complete etching of the Pt(Ni) and Pt(Co) coatings and were then polished on emery paper and subsequently on alumina powder of 0.1 and 0.01 μm particle size (Buehler).

3. Results and discussion

3.1. Microscopic (SEM), spectroscopic (EDS) and crystallographic (XRD) characterisation of the Pt(Ni) and Pt(Co) coatings

Fig. 1(A) and (B) shows the SEM micrographs of Pt(Ni) and Pt(Co) layers on a GC substrate, prepared by the electrodeposition of 308 mC cm^{-2} Ni and 353 mC cm^{-2} Co and subsequent immersion in the chloroplatinic solution, and followed by electrochemical activation in acid between hydrogen and oxygen evolution. The micrographs show rather evenly distributed deposits, characterized by a nanoparticulate structure and decorated by some uncoated areas or nanopores (for a collection of similar SEMs and a more detailed picture, the reader is referred to Ref. [31] and references therein). The roughened and particulate morphology of the platinized layers (as opposed to their smooth Ni and Co precursors [31]) may result from uneven local exchange rates of Ni or Co for Pt and the subsequent electrochemical etching of unreacted/unprotected areas. EDS analysis gave an atomic percentage composition for Pt and Ni equal to 81–19% in Pt(Ni) and for Pt and Co equal to 78–22% in Pt(Co). (The few white particles in the case of the Pt(Co) deposit of Fig. 1(B) are most likely remaining Co oxides or hydroxides (following the excursion of the electrode potential to positive potentials during electrochemical pre-treatment) since EDS analysis showed that they are rich in Co and O.)

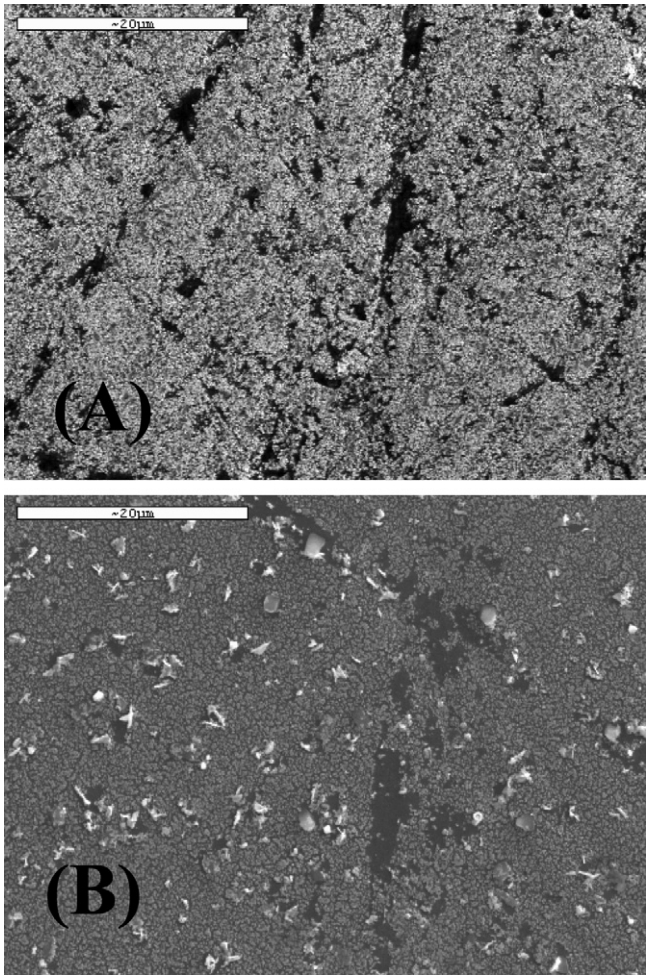

Fig. 1. SEM micrographs of (A) Pt(Ni) coating prepared by electrodeposition of a Ni layer (at a 308 mC cm^{-2} charge density) on a glassy carbon (GC) substrate, followed by partial exchange for Pt upon 30 min immersion in a 0.1 M HCl + 10^{-3} M K_2PtCl_6 solution; (B) Pt(Co) coating prepared by electrodeposition of a Co layer (at a 353 mC cm^{-2} charge density) on a glassy carbon (GC) substrate, followed by partial exchange for Pt as described above.

Fig. 2 presents an indicative grazing incidence X-ray diffractogram (GIXRD) of a thin Pt(Ni) film on a GC substrate where the pure Pt (1 1 1) and Ni(1 1 1) peak positions are also shown (according to files 04-0784 and 04-0802, JCPDS, International Center for Diffraction Data, Swarthmore, PA (2001)). The main features of the diffractogram (including the large peak at $2\theta \approx 25^\circ$ and $2\theta \approx 43^\circ$) belong to the glassy carbon substrate but the peak at $2\theta = 40.05^\circ$

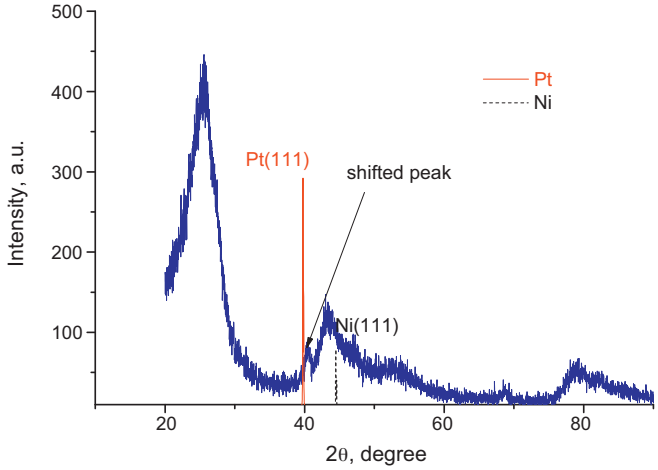

Fig. 2. Grazing-incidence XRD pattern of a Pt(Ni) coating on a GC substrate, similar to that of Fig. 1(A) above.

can be ascribed to Pt (1 1 1). The shift of this peak to values higher than the $2\theta = 39.76^\circ$ value expected for pure Pt is indicative of the entrance of a metal with a smaller lattice parameter (Ni) into the Pt lattice. A quantitative treatment of this shift according to Vegard's law [40] gives a bulk composition for a Pt–Ni alloy of 82.83–17.17%; this is very close to the 81–19% composition found by EDS and points to complete alloy formation. An analysis of the Pt-assigned peak at $2\theta = 68.60^\circ$ by the Scherrer equation gives an estimate of crystallite size as 7.29 nm.

3.2. Surface electrochemistry of Pt(Ni)/GC and Pt(Co)/GC electrodes in acid

In order to confirm that the Pt(Ni) and Pt(Co) deposits used in this work had indeed a pure Pt outer shell (in line with the findings of our previous studies, see for example [19,29–31]) and also to estimate the electroactive surface area of the electrodes, potential sweep voltammograms were recorded in a deaerated 0.1 M $HClO_4$ solution. Fig. 3 presents such voltammograms and the characteristic features of Pt surface electrochemistry (hydrogen adsorption/desorption, surface oxide formation/surface oxide stripping peak) are readily seen. The shift of the hydrogen adsorption cathodic peaks as well as that of the onset of hydrogen evolution to more negative potentials at Pt(Ni) and Pt(Co) electrodes has already been observed in the past [31,41] and has been interpreted by means of reduced adsorption affinity of these electrodes for atomic hydrogen; the shift of the formation and striping

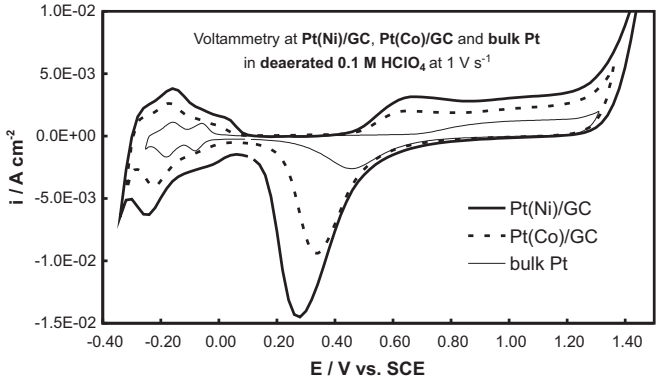

Fig. 3. Voltammograms of Pt(Ni)/GC, Pt(Co)/GC and bulk Pt disc electrodes in a deaerated 0.1 M $HClO_4$ solution at 1 V s^{-1} potential scan rate.

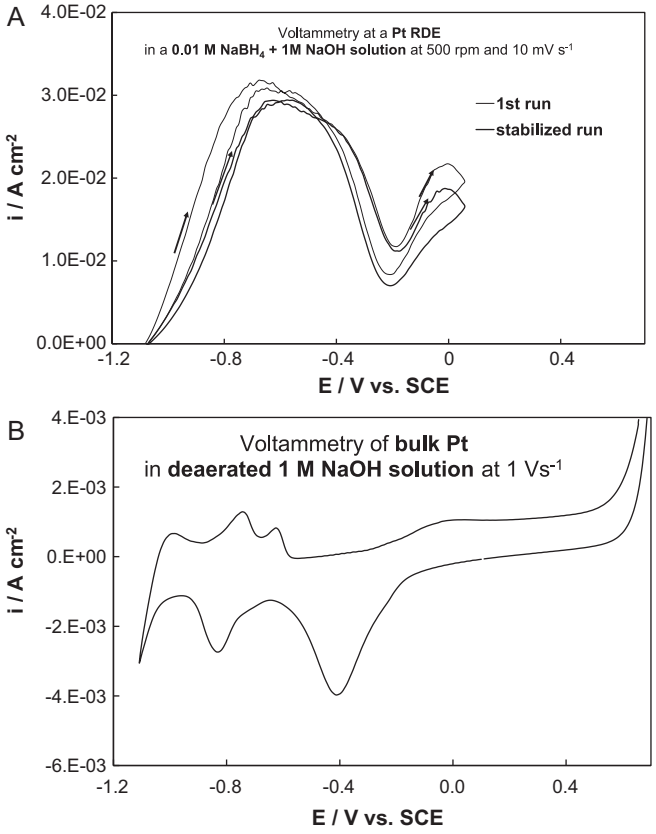

Fig. 4. (A) Initial and steady-state voltammograms (at 10 mV s^{-1} potential scan rate) of a Pt RDE in a 0.01 M $NaBH_4$ + 1 M NaOH solution, recorded at a 500 rpm rotation speed and with the start potential being the negative limit of the extended potential window studied (Stabilized as well as negative-going (reverse) runs correspond to curves at higher potentials). (B) Voltammogram of a bulk Pt disc electrode in a deaerated 1 M NaOH solution at 1 V s^{-1} potential scan rate.

peaks of Pt–O surface species to more negative potentials has also been reported but its interpretation is not clear and conflicting results have appeared in the literature (see Ref. [41] and discussion and references therein).

From the charge calculated for hydrogen adsorption and the reported value associated with a complete H monolayer [42], the electroactive area of the Pt(Ni) and Pt(Co) electrodes shown were estimated as 3.6 and 2.6 $cm^2\ cm^{-2}$, respectively. These values are in line with the set of measurements presented in [31] for similar electrodes and indicate a high degree of nanoparticle agglomeration.

3.3. Borohydride oxidation at a Pt RDE

Fig. 4(A) shows the first and steady-state voltammograms (usually the second or third in a series of successive runs) recorded at a Pt RDE in a 0.01 M $NaBH_4$ + 1 M NaOH solution, at a 500 rpm rotation speed and with special precautions taken so that at the negative potential limit (which coincides with the start potential) no cathodic hydrogen evolution/cathodic current is observed. Several remarks can be made even at a first glance. First, it is evident that there is a significant change in the electrocatalytic activity between the initial and the following scans (as well as between the forward and reverse scans), indicative of the involvement of a surface state sensitive step, as it is indeed the case of both dissociative chemisorption according to (6) and heterogeneous hydrolysis according to (10) leading to molecular hydrogen evolution. Second, preliminary Tafel plot analysis of the foot of the oxidation waves gave Tafel slope values higher than 100 mV, excluding the pos-

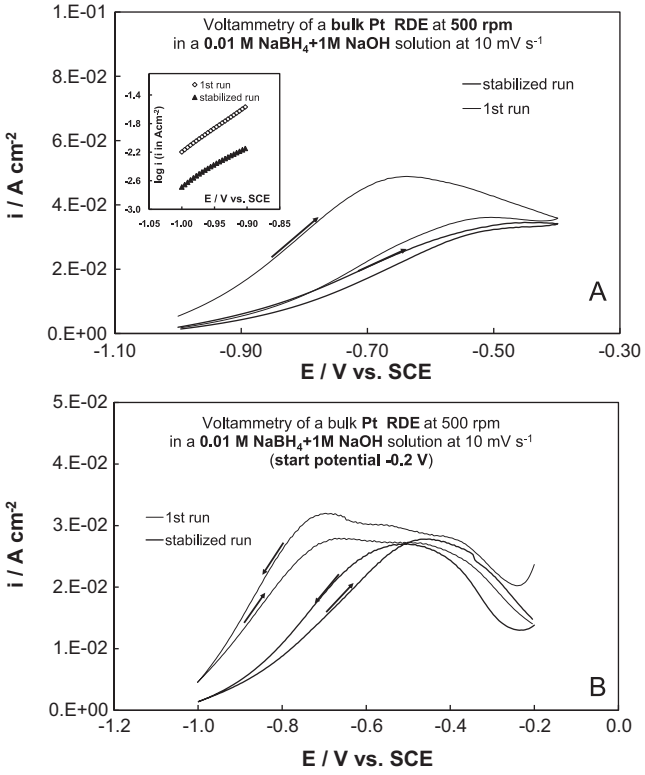

Fig. 5. (A) Initial and steady-state voltammograms (at 10 mV s^{-1} potential scan rate) of a Pt RDE in a 0.01 M $NaBH_4$ + 1 M NaOH solution, recorded at a 500 rpm rotation speed and with the start potential being the more negative limit of the narrow potential window studied (Stabilized as well as negative-going (reverse) runs correspond to curves at higher potentials). Inset: Tafel plots based on the positive-potential-sweep parts of the voltammograms. (B) Same as above but with the start potential being the less negative limit of the studied potential window.

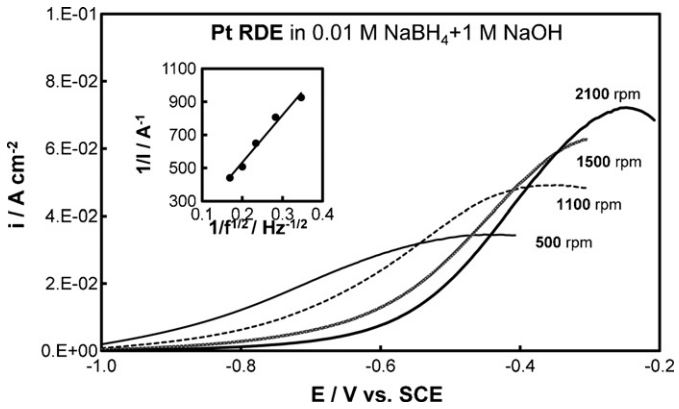

Fig. 6. Voltammograms (positive-potential-sweep scans at 10 mV s^{-1}) of a Pt RDE electrode at various rotation speeds (as indicated on the graph). Inset: Koutecky–Levich plot at −0.4 V vs. SCE.

sibility that (even at low overpotentials) the partial oxidation of the hydrolysis byproduct of BH_3OH^- [5,10,14–16] dominates the current response. Third, there is a gradual current decrease with potential, beyond the maximum observed at −0.7 to −0.6 V and down to a minimum value observed at ca. −0.2 V, following which the current partially recovers. A correlation of borohydride oxidation currents with the state of Pt surface can be attempted based on the fast voltammetry in the supporting electrolyte shown in Fig. 4(B). The latter reveals that the current fall starts after the H adsorbed monolayer is completely stripped during the anodic scan (at ca. −0.55 V), confirming the fundamental role of atomic hydrogen in borohydride oxidation on Pt, according to reactions (6) and/or (10) above. The potential range of H atom desorption/low adsorption affinity is expected to be linked to decreased borohydride activity too since the latter involves one or more steps of H adsorption, according to any of the possible paths described by the equations (6)–(10). Interestingly enough the current starts to increase again only after the Pt surface oxides start to form at potentials more positive than ca. −0.2 V. However, it seems that further increase in surface oxide coverage during the anodic scan finally leads to a new current decrease (at potentials more positive than ca. 0 V); only after the onset of oxide striping at ca. −0.3 V during the cathodic scan does the current start to rise again. We believe that most of the hysterisis phenomena between the anodic and cathodic scans of borohydride oxidation voltammograms can be explained by changes of the Pt surface state during the potential sweep experiments.

Fig. 5(A) depicts the initial and stabilized voltammetric responses of a Pt RDE electrode at 500 rpm, in a narrower potential range (with the starting potential being its more negative limit, i.e. −1.00 V). The deactivation of the electrode between the first and subsequent runs is observed again, excluding the possibility of its origin being the exposure in the double layer and oxide formation regions (as in the case of Fig. 4(A)). Fig. 5(B) shows voltammograms where the start potential was the less negative value of the potential window (−0.20 V). It is seen that the shape, location and magnitude of the first set of voltammetric curves of Fig. 4(A) (start potential at more negative values) and Fig. 5(B) (start potential at less negative values) are similar. It seems therefore that the apparent change in electrode activity (aging) is not due to the formation of a film comprising of insoluble borohydride oxidation products at positive potentials/oxidation rates, as has been postulated in some cases [10]. The inset in Fig. 5(A) shows the Tafel plots of the positive going (forward) scans of the two voltammograms in the −1.00 to −0.90 V range; good linearity is observed and Tafel slope values of 156 and 200 mV per decade are estimated for the initial and final voltammograms, respectively. These values are higher than the 120 mV expected for hydrogen oxidation on Pt following the Volmer–Heyrovsky mechanism at moderate overpotentials (see for example the recent Refs. of [43,44] and references therein) but lower than values as high as 340 mV reported in the case of direct multi-electron oxidation of BH_4^- or BH_3OH^- via the reaction series of (7). It seems therefore that in the experiments of Fig. 5(A) borohydride is oxidized at low overpotentials by both routes, i.e. both the oxidation of hydrogen produced by its fast heterogeneous hydrolysis and by its direct electron loss. Deactivation of the electrode between its initial and final voltammogram can be attributed to a loss of its hydrolysis/hydrogen production activity that shifts the curve to more positive potentials and increases the Tafel slope.

Fig. 6 presents the stabilized-steady state positive potential sweep voltammograms for borohydride oxidation obtained at various rotation rates at a Pt RDE. There is a very large shift of the voltammograms to positive potentials with electrode rotation rate, as well as the disappearance of a well-defined plateau, unlike the results presented in Refs. [10,38] for Pt but similar to those of [19]. There are, however, significant differences between the experiments presented in this work and those of Refs. [10,38]. In Ref. [10] the initial curves were shown and the potential was negative enough so that cathodic hydrogen evolution took place at the start potential. The hydrogen thus evolved could be oxidized once the potential became more positive the rest potential during the anodic scan; also, as mentioned in the discussion of Fig. 4 above, electrode cathodization apparently increases the activity of Pt for hydrogen production via heterogeneous borohydride hydrolysis. In Ref. [38], although the start potential seems to have been chosen carefully enough to avoid cathodic hydrogen evolution, the reported results still correspond to the initial voltammetric run

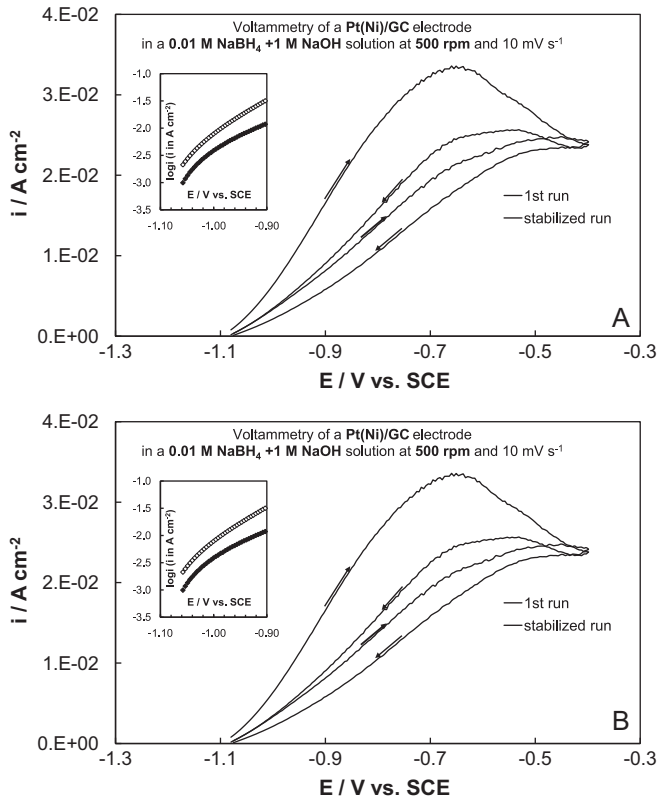

Fig. 7. (A) Initial and steady-state voltammograms (at 10 mV s^{-1} potential scan rate) of a Pt(Ni)/GC RDE in a 0.01 M $NaBH_4$ + 1 M NaOH solution, recorded at a 500 rpm rotation speed and with a start potential being the more negative limit of the studied potential window (Stabilized as well as negative-going (reverse) runs correspond to curves at higher potentials). Inset: Tafel plots based on the positive-potential-sweep parts of the voltammograms. (B) Same as above but for a Pt(Co)/GC RDE.

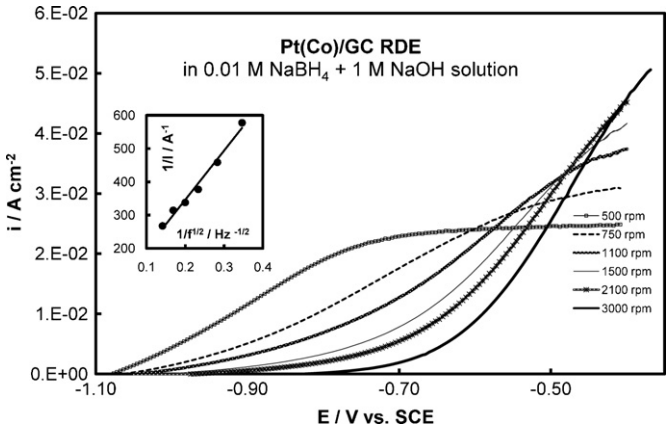

Fig. 8. Voltammograms (positive-potential-sweep scans at 10 mV s^{-1}) of a Pt(Co)/GC RDE electrode at various rotation speeds (as indicated on the graph). Inset: Koutecky–Levich plot at–0.4 V vs. SCE.

which reflects (according to our findings too) an activated surface. These differences stress the importance of experimental details in accessing the activity for borohydride oxidation via voltammetric measurements. In the case of stabilized voltammograms with a start potential positive to the rest potential as those of Fig. 6, the large shift of the half-wave potential to more positive values as the rotation speed of the electrode increases indicates a highly irreversible reaction. This can be due to the products of heterogeneous hydrolysis (BH_3OH^- and H_2, see reaction (10)) or/and the soluble intermediates of direct borohydride oxidation (see reaction (7)) transported away from the electrode before they are oxidized. The inset shows the corresponding Koutechky–Levich plot at −0.4 V vs. SCE from which the apparent number of electrons involved in borohydride oxidation can be estimated. The diffusion coefficient of borohydride was taken as $D = 1.85 \times 10^{-5}$ cm^2 s^{-1}, calculated from the Koutechky–Levich equation applied to the results obtained at a bulk Au RDE [19] and assuming that the reaction proceeds at this electrode material via the loss of $8e^-$ [5–7,9]. This value for D is similar to the one reported in Ref. [45] (1.68×10^{-5} cm^2 s^{-1}). We thus estimated the value of $n_{app} = 5.6$ for the bulk Pt RDE. This is within the wide 3–6 electrons range that usually appears in the literature for this metal [6,13] and indicates that at high overpotential values borohydride oxidation at Pt proceeds via the direct 4e oxidation mechanism of reactions (7) accompanied by the partial oxidation of the atomic hydrogen produced (reaction (9)).

3.4. Borohydride oxidation at Pt(Ni)/GC and Pt(Co)/GC RDEs

Fig. 7(A) and (B) depicts the initial and stabilized voltammetric responses of Pt(Ni)/GC and Pt(Co)/GC RDE electrodes at 500 rpm, in a 0.01 M $NaBH_4$ + 1 M NaOH solution. The first noticeable difference between the bimetallic electrodes and the plain Pt one is that the apparent change in their initial activity is not as pronounced and neither is the difference between the forward and backward scans (especially in the case of Pt(Co)). The insets show the corresponding Tafel plots for the positive going parts of the voltammograms (after mass transfer correction).

The mass-transfer-corrected (kinetic) current density $i_{(k)}$ was calculated from the measured $i_{(total)}$ value by the standard $1/i_{(total)} = 1/i_{(k)} + 1/i_L$ formula (where i_L is the limiting current and which becomes the Koutecky–Levich equation for the RDE electrode [38]).

Two linear regions could be identified and the one at low overpotentials (−1.06 V to −1.00 V) has, in the case of the stabilized response, a Tafel slope of 100 mV and 97 mV for Pt(Ni) and Pt(Co), respectively; in the higher overpotentials range of −1.00 V to −0.90 V these values are 176 mV and 202 mV (similar to those of Pt). This means that at the negative potentials below −1.00 V accessible with the bimetallic electrodes (see also discussion below) borohydride proceeds primarily by the oxidation of molecular hydrogen produced by heterogeneous hydrolysis while the competing mechanism of direct borohydride oxidation starts to occur at potentials less negative than −1.00 V.

Fig. 8 shows RDE experiments at various rotation rates of a Pt(Co)/GC electrode and the same very large shift of the half-wave potential as for Pt electrodes is observed, for reasons similar to those holding for Pt and presented in the discussion of Fig. 6. However, the Koutecky–Levich analysis based on the plot shown in the inset of the same figure, gives the apparent number of electrons transferred as $n_{app} = 4.3$ (similar results were obtained for Pt(Ni)) meaning that at bimetallic electrodes the direct 4e (partial) oxidation mechanism dominates at high overpotentials and that hydrogen oxidation is limited in the same potential range.

Fig. 9(A) compares the voltammograms of the three types of electrodes tested (i.e. Pt, Pt(Ni)/GC and Pt(Co)/GC) in a 0.01 M $NaBH_4$ + 1 M NaOH solution at the lowest rotation rate studied (500 rpm). The first point that one has to make is that the rest potential of the Pt(Ni) and Pt(Co) electrodes was measured as −1.15 and −1.10 V, respectively, as opposed to the −1.04 V value found for Pt. This can be explained by the fact that the rest potential is determined by the intercept of the Tafel lines of borohydride or/and hydrogen byproduct oxidation and that of cathodic hydrogen evolution. If the latter process is hindered or/and the former process enhanced, then the rest potential shifts to more positive values. The suppression of cathodic hydrogen evolution at Pt(Co) and Pt(Ni) electrodes with respect to Pt has already been con-

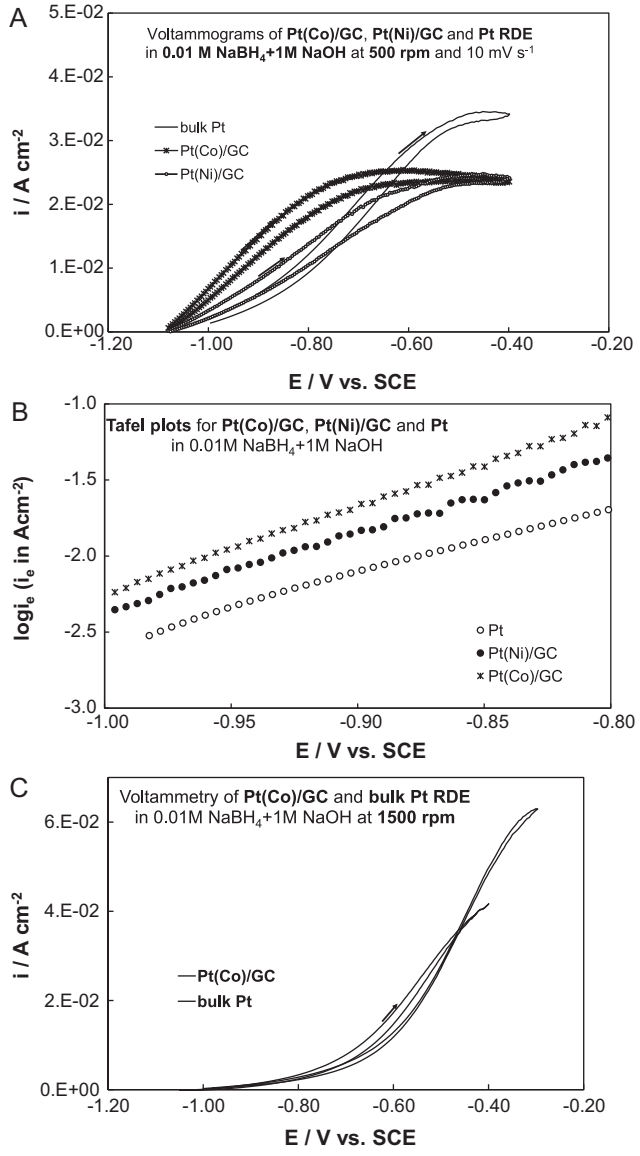

Fig. 9. (A) Steady-state voltammograms (recorded at 500 rpm rotation speed and a 10 mV s^{-1} potential scan rate) of Pt(Ni)/GC, Pt(Co)/GC and bulk Pt RDEs in 0.01 M $NaBH_4$ + 1 M NaOH solutions, with a start potential being the more negative limit of the studied potential window. (B) Tafel plots based on the positive-potential-sweep parts of the voltammograms of (A) above. (C) Steady-state voltammograms of a Pt(Co)/GC and a bulk Pt RDE in 0.01 M $NaBH_4$ + 1 M NaOH solutions at 1500 rpm rotation speed and a 10 mV s^{-1} potential scan rate (start potential is the more negative limit of the studied potential window); the Pt(Co) voltammogram corresponds to curves at lower potentials).

firmed experimentally [31]. It has been interpreted by taking into account the Pt d-band energy center (ε_d) downshift in the presence of Cu, Fe, Co, Ni (i.e. metals with a smaller Wigner–Seitz radius and electronegativity than Pt), as predicted theoretically by DFT calculations [32,33]. This in turn decreases Pt adsorption affinity for hydrogen (both atomic and molecular). Since pure Pt has the optimum Pt–H bond strength for cathodic hydrogen evolution, any change of this strength would lead to a decrease in the reaction rate. This allows the potential to be made ca. 100 mV more negative at the bimetallic electrodes than at pure Pt without cathodic hydrogen evolution commencing-negative currents observed. It therefore ensures the oxidation of molecular hydrogen produced by hydrolysis of borohydride (reactions (10); see also the Tafel slope values from Fig. 7) without the competing direct borohydride oxidation (reaction (7)) occurring at these low potentials (−1.10 to −1.00 V range). The second observation is that among the two bimetallic electrodes (showing similar rest potentials and hence similar accessible potential windows), Pt(Co) appears to be superior to Pt(Ni); this may be attributed to either being more active towards the hydrolysis reaction (10) or towards the oxidation of generated molecular hydrogen which, according to the Tafel slope found above (ca. 100 mV), proceeds via:

$$Pt + H_2 + OH^- - e^- \rightarrow Pt\text{–}H + H_2O \quad (13.1)$$

$$Pt\text{–}H + OH^- - e^- \rightarrow Pt + H_2O \quad (13.2)$$

According to Refs. [32,33] Co has a stronger ε_d and adsorption affinity lowering effect on Pt than Ni and as a result the Pt–H needed for the onset of hydrolysis according to (10.1) is weaker at Pt(Co) than Pt(Ni). This means that a change in hydrolysis activity is unlikely to be the origin of the different currents observed since it would lead to a trend opposite to that observed. On the contrary, the molecular H_2 de-electronation according to (13.1) would be favoured by a weak Pt–$(H_2)_{ads}$ bond that would allow easy release of a proton into the solution.

In the intermediate potential range (above −1.00 V and below the onset of pure mass transfer control and associated limiting current) both indirect (via hydrogen oxidation) and direct borohydride oxidation are expected to occur, as indicated by the values of Tafel slopes estimated from the voltammograms of Fig. 7. An accurate comparison of electrode activity at these potentials requires correction for mass transfer effects and electroactive surface area (esa) differences. Fig. 9(B) shows mass-transfer-corrected Tafel plots with current densities expressed per esa, i.e. Pt(Co) is found again to be superior than Pt(Ni) and the latter better than pure Pt. This trend can be interpreted too (according to the reasoning presented above) by higher rates of H_2 oxidation at Pt(Co) and Pt(Ni) electrodes and is further confirmed by the results shown in Fig. 9(C) whereby at increased electrode rotation rates (1500 rpm) the bimetallic and pure Pt electrodes have similar currents in the kinetic and mixed control potential range. If the differences observed between different electrodes are due to differences in H_2 oxidation rates then, when the latter is lost into the solution at high rotation rates, their catalytic activity should be similar, as indeed is the case.

Finally, according to the voltammetric picture in the mass transfer control potential range, the Pt(Ni) and Pt(Co) electrodes exhibit lower limiting currents for borohydride oxidation than Pt, in line with n_{app} values of ca. 4 for the bimetallic electrodes and of ca. 5.5 for Pt estimated above. Since in that potential range borohydride oxidation at Pt-based electrodes proceeds predominantly by the (partial) direct oxidation route described by reaction (7), the only way that n_{app} can exceed the value of 4 is that of the strongly adsorbed atomic hydrogen M–H intermediate to be further oxidized according to reaction (9). When weaker M–H bonds are formed as is the case of Pt(Co) and Pt(Ni) then molecular hydrogen is produced instead according to the recombination reaction (8). Contrary to the situation at lower potentials, the significant rates of borohydride oxidation at high potentials and the associated high coverage in the boron-containing intermediates of (7) hinders molecular H_2 oxidation which is lost into the solution.

4. Conclusions

(a) Careful choice of the negative potential limit of cyclic voltammetry experiments at a Pt RDE, positive to the rest potential in a 0.01 M $NaBH_4$ + 1 M NaOH solution, revealed a gradual decrease in current response with number of voltammogram run until a steady-state picture is achieved, irrespective of initial scan direction. This could be associated with a change in heterogeneous borohydride hydrolysis and/or oxidation rates of thus produced molecular hydrogen. The significant shift of

the voltammograms upon increased rotation rates to more positive potentials is characteristic of a highly irreversible reaction while the apparent number of electrons (n_{app}) lost by borohydride at high overpotentials is estimated as 5.6 indicating the simultaneous borohydride 4e direct oxidation and that of adsorbed atomic hydrogen.

(b) Cyclic voltammetry of bimetallic Pt(Ni)/GC and Pt(Co)/GC RDEs (prepared by spontaneous galvanic replacement of Ni and Co electrodeposits upon their immersion in a chloroplatinic acid) was similar to that of pure Pt. Since the rest potential of Pt(Co) and Pt(Ni) was more negative than that of Pt (due to a suppression of cathodic hydrogen evolution), access to lower overpotentials was allowed and the catalytic activity of Pt(Co) and Pt(Ni) in the kinetic and mixed control potential range was found to be higher than that of pure Pt. This is attributed to a higher activity of these electrodes for oxidation of molecular hydrogen produced by heterogeneous hydrolysis at low overpotentials. However, the apparent number of electrons exchanged during borohydride oxidation in the limiting plateau-mass transfer control potential range has been estimated to be lower at Pt(Ni) and Pt(Co) electrodes (ca. 4) due to the escape of molecular hydrogen to the solution during increased borohydride direct oxidation rates.

Acknowledgements

ΓΓΕΤ Greece for ΠΕΝΕΔ-03ΕΔ378 Project and a scholarship to A.T. Ministry of Education, Greece for an "ΗΡΑΚΛΕΙΤΟΣ" scholarship to I.M.

References

[1] R.L. Pecsok, J. Am. Chem. Soc. 75 (1953) 2862.
[2] M.E. Indig, R.N. Snyder, J. Electrochem. Soc. 109 (1962) 1104.
[3] J.P. Elder, A. Hickling, Trans. Faraday Soc. 58 (1962) 1852.
[4] J.H. Morris, H.J. Gysling, D. Reed, Chem. Rev. 85 (1985) 51.
[5] M.V. Mirkin, H. Yang, A.J. Bard, J. Electrochem. Soc. 139 (1992) 2212.
[6] C. Ponce de Leon, F.C. Walsh, D. Pletcher, D.J. Browning, J.B. Lakeman, J. Power Sources 155 (2006) 172.
[7] U.B. Demirci, J. Power Sources 172 (2007) 676.
[8] U.B. Demirci, P. Miele, C.R. Chimie 12 (2009) 943–950.
[9] E. Gyenge, Electrochim. Acta 49 (2004) 965.
[10] B. Molina Concha, M. Chatenet, Electrochim. Acta 54 (2009) 6119.
[11] J.I. Martins, M.C. Nunes, R. Koch, L. Martins, M. Bazzaoui, Electrochim. Acta 52 (2007) 6643.
[12] J.I. Martins, M.C. Nunes, J. Power Sources 175 (2008) 244.
[13] B.H. Liu, Z.P. Li, S. Suda, Electrochim. Acta 49 (2004) 3097.
[14] J.A. Gardiner, J.W. Collat, J. Am. Chem. Soc. 86 (1964) 3165.
[15] J.A. Gardiner, J.W. Collat, J. Am. Chem. Soc. 87 (1965) 1692.
[16] J.A. Gardiner, J.W. Collat, Inorg. Chem. 4 (1965) 1208.
[17] E. Gyenge, M.H. Atwan, D.O. Northwood, J. Electrochem. Soc. 153 (2006) A150.
[18] K. Wang, K. Jiang, J. Lu, L. Zhuang, C. Cha, X. Hu, G.Z. Chen, J. Power Sources 185 (2008) 892.
[19] A. Tegou, S. Armyanov, E. Valova, O. Steenhaut, A. Hubin, G. Kokkinidis, S. Sotiropoulos, J. Electroanal. Chem. 634 (2) (2009) 104–110.
[20] C. Celik, F.G.B. San, H.I. Sarac, Int. J. Hydrogen Energy 35 (2010) 8678.
[21] A.J. Bard, R. Parsons, J. Jordan (Eds.), Standard Potentials in Aqueous Solution, Marcel Dekker Inc., NY/Basel, 1985.
[22] S.R. Brankovic, J.X. Wang, R.R. Adzic, Surf. Sci. 474 (2001) L173.
[23] M. Van Brussel, G. Kokkinidis, I. Vandendael, C. Buess-Herman, Electrochem. Commun. 4 (10) (2002) 808.
[24] K. Sasaki, Y. Mo, J.X. Wang, M. Balasubramanian, F. Uribe, J. McBreen, R.R. Adzic, Electrochim. Acta 48 (2003) 3841.
[25] M. Van Brussel, G. Kokkinidis, A. Hubin, Cl. Buess-Herman, Electrochim. Acta 48 (2003) 3909.
[26] J. Zhang, M.B. Vukmirovic, K. Sasaki, A.U. Nilekar, M. Mavrikakis, R.R. Adzic, J. Am. Chem. Soc. 127 (2005) 12480.
[27] M.B. Vukmirovic, J. Zhang, K. Sasaki, A.U. Nilekar, F. Uribe, M. Mavrikakis, R.R. Adzic, Electrochim. Acta 52 (2007) 2257.
[28] R.R. Adzic, J. Zhang, K. Sasaki, M.B. Vukmirovic, M. Shao, J.X. Wang, A.U. Nilekar, M. Mavrikakis, J.A. Valerio, F. Uribe, Top. Catal. 46 (2007) 249.
[29] S. Papadimitriou, A. Tegou, E. Pavlidou, G. Kokkinidis, S. Sotiropoulos, Electrochim. Acta 52 (2007) 6254.
[30] A. Tegou, S. Papadimitriou, E. Pavlidou, G. Kokkinidis, S. Sotiropoulos, J. Electroanal. Chem. 608 (2007) 67.
[31] S. Papadimitriou, A. Tegou, E. Pavlidou, E. Valova, S. Armyanov, G. Kokkinidis, S. Sotiropoulos, Electrochim. Acta 53 (22) (2008) 6559.
[32] A. Ruban, B. Hammer, P. Stoltze, H.L. Skriver, J.K. Nørskov, J. Mol. Catal. A: Chem. 115 (1997) 421.
[33] J.R. Kitchin, J.K. Nørskov, M.A. Barteau, J.G. Chen, J. Chem. Phys. 120 (21) (2004) 10240.
[34] M. Chatenet, F. Micoud, I. Roche, E. Chainet, Electrochim. Acta 51 (2006) 5459.
[35] H. Cheng, K. Scott, Electrochim. Acta 51 (2006) 3429.
[36] M.H. Atwan, C.L.B. Macdonald, D.O. Northwood, E.L. Gyenge, J. Power Sources 158 (2006) 36.
[37] M. Chatenet, B. Molina Concha, N. El-Kissi, G. Parrour, J.-P. Diard, Electrochim. Acta 54 (2009) 4426.
[38] D.A. Finkelstein, N. Da Mota, J.L. Cohen, H.D. Abruna, J. Phys. Chem. C 113 (2009) 19700.
[39] W.D. Callister Jr., Materials Science Engineering: An Introduction, fourth ed., John Wiley and Sons, Inc., New York, 1997.
[40] A.R., West in Basic Solid State Chemistry, second ed., John Wiley and Sons Ltd., Chichester, 1999.
[41] A. Tegou, S. Papadimitriou, G. Kokkinidis, S. Sotiropoulos, J. Solid State Electrochem. 634 (2009) 104.
[42] H. Kita, H. Nakajima, Electrochim. Acta 31 (2) (1986) 193.
[43] P.M. Quaino, M.R.G. De Chialvo, A.C. Chialvo, Electrochim. Acta 52 (2007) 7396.
[44] S.A. Vilekar, I. Fishtik, R. Datta, J. Electrochem. Soc. 157 (7) (2010) B1040.
[45] G. Denuault, M.V. Mirkin, A.J. Bard, J. Electroanal. Chem. 308 (1991) 27.